ratio reaches a peak value of about 28% at 900 kev. In the high-energy limit, however, $G(n,\rho)$ vanishes and the ratio is just a ratio of two constants and will no longer be energy dependent. We then have

$$\left.\frac{\frac{1}{2}\sigma_{\mathrm{MBK}^-}}{\frac{1}{2}\sigma_{\mathrm{MBK}^+}}\right|_{v\to\infty} \to \frac{[(\Delta_{im}-\chi_{im})(1-c)]^2(1+\Delta_i)}{[(\Delta_{im}+\chi_{im})(1+c)]^2(1-\Delta_i)}. \quad (29)$$

For the Wang wave function, the ratio at the high-energy limit is about 19%; for the Weinbaum, about 7%. Figure 4 shows a plot of this ratio against energy. Curve *I* is plotted for the Wang wave function; curve *II* for the Weinbaum; the straight lines *A* and *B* indicate, for the Wang and Weinbaum, respectively, the high-energy limit ratios computed from Eq. (29). The maximum at 900 kev is due entirely to the fact that at this energy the destructive interference in the gerade transitions (and the corresponding constructive interference in the ungerade transitions) is most pronounced. A further increase of incident energy decreases the ratio, which thereafter oscillates slowly and with rapidly decreasing amplitude about the high-energy limit ratio.

The fact that the projection onto ungerade states of the molecular-ion is zero when we employ the extreme molecular orbital wave function can be easily understood, since the extreme molecular orbital is nothing more than a product of two gerade (extreme) molecular-ion wave functions.

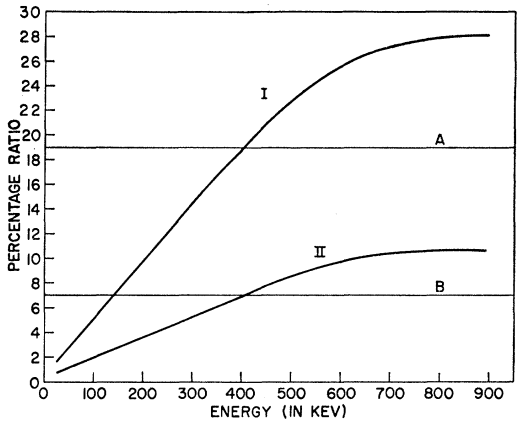

FIG. 4. The ratio of capture cross section corresponding to transition to ungerade states to the transition to gerade states. Curve *I* shows the ratio for the Wang extreme atomic orbital wave function, and curve *II* for the Weinbaum. The straight lines *A* and *B* indicate the high-energy limit cross-section ratios for the Wang and the Weinbaum wave functions, respectively.

The results which have been quoted in this section remain essentially unaltered when $\sigma_{\mathrm{MJS}}{}^{\pm}$ are substituted for $\sigma_{\mathrm{MBK}}{}^{\pm}$.

ACKNOWLEDGMENTS

We are indebted to Dr. Richard M. Drisko, Dr. T. M. Donahue, and Dr. Robert H. Bassel for many helpful discussions.

PHYSICAL REVIEW VOLUME 117, NUMBER 3 FEBRUARY 1, 1960

Photodisintegration of the Deuteron with 94-Mev Bremsstrahlung Radiation*†

J. A. GALEY‡
The Enrico Fermi Institute for Nuclear Studies, The University of Chicago, Chicago, Illinois
(Received August 24, 1959)

Differential cross sections for the reaction $\gamma+d\to p+n$ have been determined at laboratory angles of 45°, 75°, 90°, and 135° for laboratory photon energies from approximately 50 to 90 Mev. At each of the above angles the energy spectrum of the recoil protons was determined with a counter telescope and a pulse-height analysis system. The low cross section for this reaction necessitates the reduction of background to a minimum. This was accomplished by the use of a gaseous target and a particle selection technique. The differential cross sections and the estimates of the parameters describing angular distributions are in reasonable agreement with recent calculations by de Swart and Marshak and by Zernik, Rustgi, and Breit.

I. INTRODUCTION

ALONG with single and multiple nucleon-nucleon scattering and the *n-p* capture process, the photodisintegration of the deuteron constitutes a possible source of information on two-body nuclear interactions. It is unique in the photonuclear field, because the matrix elements describing the process are more readily calculated than those involved in gamma-ray interactions with more complex nuclei. In addition, being a two-body interaction the determination of the energy and the angle of recoil of the proton (or the neutron) uniquely fixes the energy of the photon initiating the reaction.

The energy range from 20 Mev on up where effective range theory is not satisfactory has been investigated

* Research supported by a joint program of the Office of Naval Research and the U. S. Atomic Energy Commission.

† A thesis submitted to the Department of Physics, the University of Chicago, in partial fulfillment of the requirements for the Ph.D. degree. A more complete account of the method of data reduction and of sources of error is given in the thesis filed with the Department of Physics, University of Chicago.

‡ Present address: Department of Physics, University of Notre Dame, Notre Dame, Indiana.

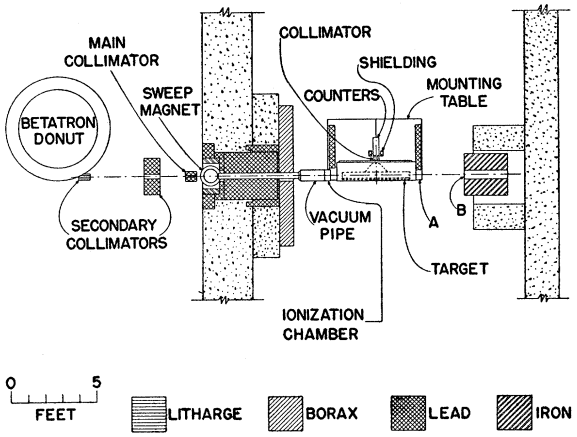

FIG. 1. A plan view of the experimental arrangement.

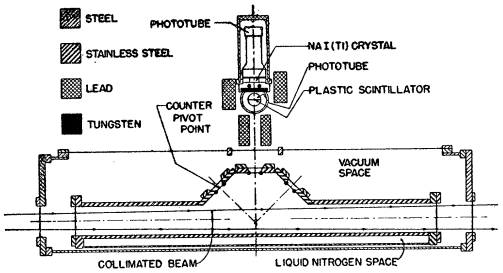

FIG. 2. A plan view of the target and counter telescope.

near 20 Mev at the University of Pennsylvania,[1,2] in the intermediate energy range at the University of Illinois[3] and at the Lebedev Physics Institute,[4] and in the high-energy range at the California Institute of Technology,[5] the University of Illinois,[6] the University of California at Berkeley,[7] and Purdue University.[8] A more comprehensive coverage of the large amount of work that has been done on the deuteron photoeffect is available in a bibliography compiled by Toms.[9]

Further information may be extracted from the study of photoprotons from deuterium by the determination of the proton polarization, though this has thus far received only theoretical attention.[10]

Section II of this paper describes the equipment used and the procedure followed in obtaining data. Section III deals with the calculation of cross sections, and Sec. IV summarizes the results and gives a comparison of these results with recent calculations.[11,12]

II. EQUIPMENT AND PROCEDURE

A plan view of the experimental arrangement is given in Fig. 1. The University of Chicago's 100-Mev betatron was used as a source of radiation. The main collimator defined a beam $2\frac{1}{2}$ inches in diameter at the center of the deuterium target. The sweep magnet and associated vacuum system provided an electron-free beam, while shielding from stray gamma radiation was provided by the lead and heavy concrete of the betatron vault wall, lead stacked on the target and counter telescope mounting table, and a beam stop which eliminated back scattered radiation. The borax shielding served to reduce the neutron flux in the experimental area.

The kinetic energy of the electrons producing the x-ray beam was maintained constant by applying to a discriminator the integral of the voltage produced in a turn of wire enclosing the flux of the betatron field. Measurement of the magnitude of the betatron guide field at the x-ray target at the time the electrons struck the target gave for the kinetic energy of the electrons the value 93.5 ± 0.5 Mev.

The time integral of the beam intensity was determined from the charge collected on the plates of an argon filled, thin, transmission-type ionization chamber. This is denoted by "ionization chamber" in Fig. 1. The charge collected on the plates of this chamber was stored on a polystyrene capacitator and the resultant voltage indicated by an Applied Physics Corporation model 301 vibrating reed electrometer.

Daily checks of the ionization chamber were made by comparison with a thimble type ionization chamber placed in the position denoted by "*B*" in Fig. 1. The use of an ionization chamber of the type described by Kerst and Edwards,[13] located in position "*A*" of Fig. 1, allowed the ionization chamber measurements to be placed on an absolute basis. The Kerst-Edwards chamber used was calibrated by the National Bureau of Standards. An upper limit of 5% is placed on the uncertainty associated with the calibration of the Kerst-Edwards chamber.[14]

Figure 2 shows in plan view the target and counter telescope. The target consisted of deuterium gas at pressures of 13 to 14 atoms in a stainless steel container of welded construction, held at 77.4°K by the use of a liquid nitrogen shell. The target volume was defined by $\frac{3}{8}$-inch tungsten rods mounted on the target and counter telescope. The counter telescope consisted of a 94 mg/cm^2 plastic scintillator and a NaI(Tl) crystal.

[1] J. Halpern and E. V. Weinstock, Phys. Rev. **91**, 934 (1953).
[2] A. L. Whetstone and J. Halpern, Phys. Rev. **109**, 2072 (1958).
[3] L. Allen, Phys. Rev. **98**, 705 (1955).
[4] Alekandrov, Delene, Solovokhotov, Sokol, and Shtarkov, J. Exptl. Theoret. Phys. U.S.S.R. **33**, 614 (1957) [translation: Soviet Phys. JETP **6**, 472 (1958)].
[5] J. C. Keck and A. V. Tollestrup, Phys. Rev. **101**, 360 (1956).
[6] Whalin, Schriever, and Hanson, Phys. Rev. **101**, 377 (1956).
[7] D. R. Dixon and K. C. Bandtel, Phys. Rev. **104**, 1730 (1956).
[8] Tatro, Palfrey, Whaley, and Haxby, Phys. Rev. **112**, 932 (1958).
[9] M. E. Toms, Bibliography No. 14 of the Naval Research Laboratory, Washington, D. C., August, 1958 (unpublished).
[10] See, for example, reference 12.
[11] J. J. de Swart and R. E. Marshak, Phys. Rev. **111**, 272 (1958); J. J. de Swart, J. Appl. Phys. **25**, 233 (1959); and J. J. de Swart (private communication).
[12] Zernik, Rustgi, and Breit, Phys. Rev. **114**, 1358 (1939).
[13] P. D. Edwards and D. W. Kerst, Rev. Sci. Instr. **24**, 490 (1953).
[14] J. S. Pruitt (private communication).

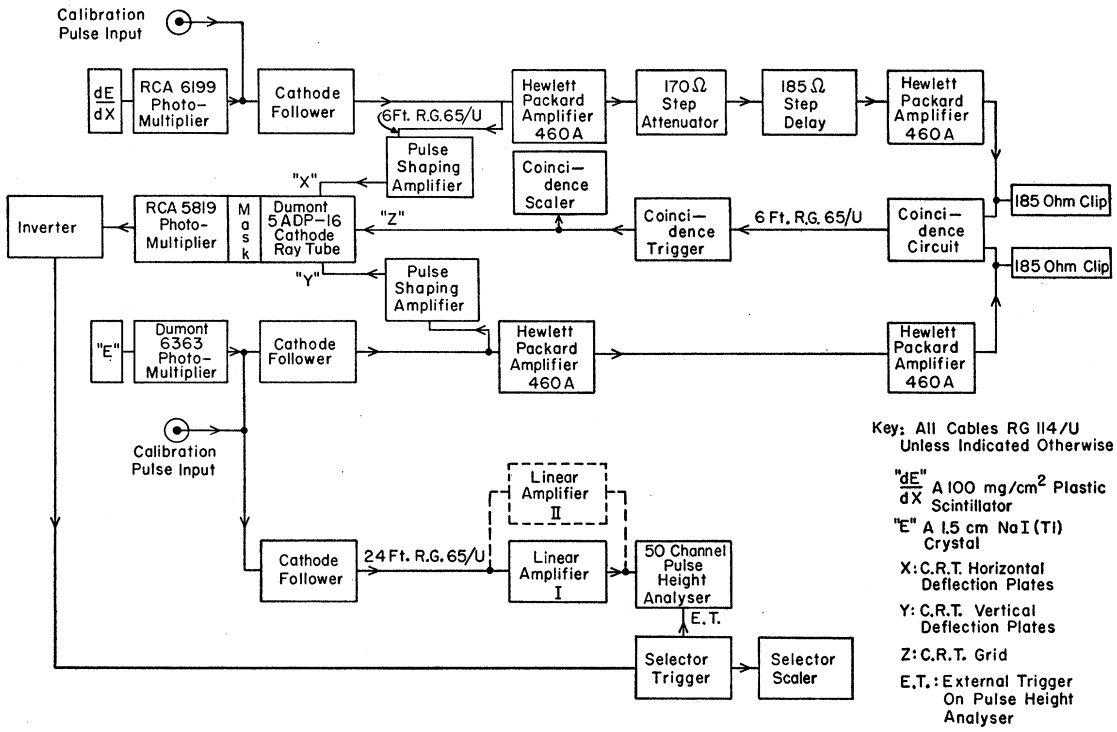

FIG. 3. A block diagram of the electronics.

It is estimated that the error in the alignment of the axis of the counter telescope with respect to the x-ray beam is less than 1°.

The electronics, shown in block diagram form in Fig. 3, served two functions: (1) the elimination of counts due to electrons, i.e., particle selection, and (2) the measurement of proton energy loss in the NaI(Tl) crystal through pulse-height analysis. The stability of the electronics was regularly checked with a precision pulser, whose wave form was a close approximation to that produced by the photomultiplier viewing the NaI(Tl) crystal, and with the gamma radiation from Cs^{137}. The extent of nonlinearities in the pulse-height analysis system was determined with the use of a sliding pulser.

The energy scale of the pulse-height analysis system was determined from the channel number on the pulse-height analyzer, corrected for nonlinearities, corresponding to known proton energies. There are two sources of information of this sort: the location of the end points of the photo-proton spectra and the pulse-height distributions observed for protons produced by magnetic analysis of the energy degraded external proton beam of the University of Chicago 450-Mev synchrocyclotron.[15] The uncertainty associated with this determination is less than 0.5%.

[15] The calibration of the analyzing magnet used during the cyclotron runs was that obtained by L. G. Pondrom, Phys. Rev. **114**, 1623 (1959). This paper also describes the external proton beam facility of the cyclotron that was employed in this experiment.

The observation of monoenergetic protons from the cyclotron also allowed a determination of the resolution of the pulse-height analysis system. Since the resolution function was symmetric the amount that the finite resolution will perturb the photoproton spectra may be estimated from the mean square width of the resolution function and the second derivative of the pulse-height spectrum. An estimate of the effect of finite resolution in the regions of the photoproton spectra where the second derivative is largest indicates that it is always considerably less than the effect of the statistical uncertainty in the number of counts per channel.

III. CALCULATION OF CROSS SECTIONS

Background

There were two major sources of background: one time dependent and one beam dependent. The former amounted to 2.5±0.20 counts per hour. The latter was determined from runs in which the target was filled with hydrogen.

Corrections and Uncertainties

The data were reduced to differential cross sections in a straightforward manner. Corrections were made for nonideal gas behavior of the deuterium, the loss of protons in traversing the materials between the target and the NaI(Tl) crystal, and the deadtime of the

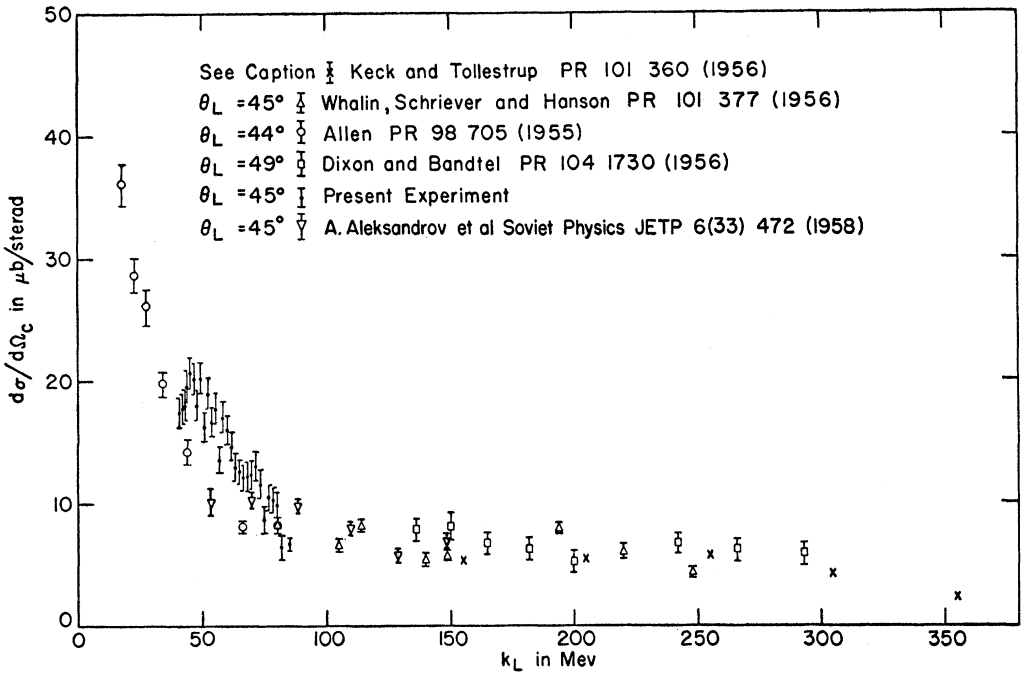

(a)

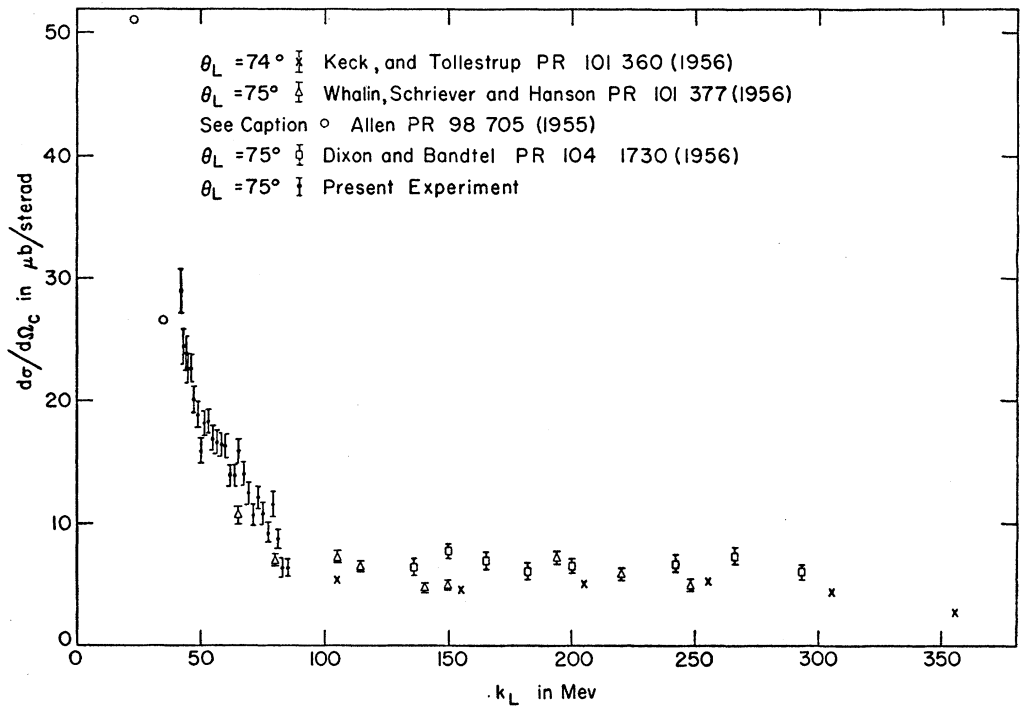

(b)

FIG. 4. A survey of experimental determinations of the differential cross section for fixed laboratory angles: (a) 45°—Keck and Tollestrup's values are the averages of their tabulated values for 39° and 56°. (b) 75°—Allen's value was taken from the smooth curve in his angular distribution plot. (c) 90°—Allen's and Whalin's values were taken from the smooth curves in their angular distribution plots. Dixon's and Bandtel's are the averages of their tabulated values for 75° and 106°. (d) 135°—Whalin, Schriever, and Hanson's values are the averages of their tabulated values for 120° and 150°. The subscripts "c" and "l" in this figure, subsequent figures, tables and the remainder of the text indicate quantities in the center-of-mass and laboratory systems, respectively.

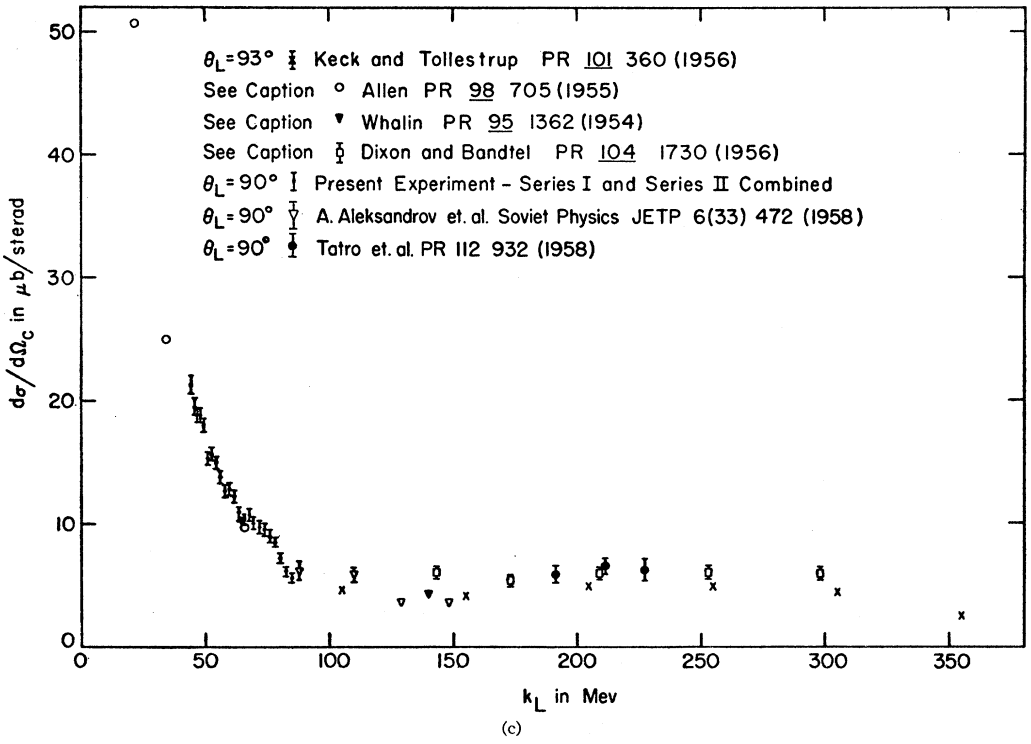

(c)

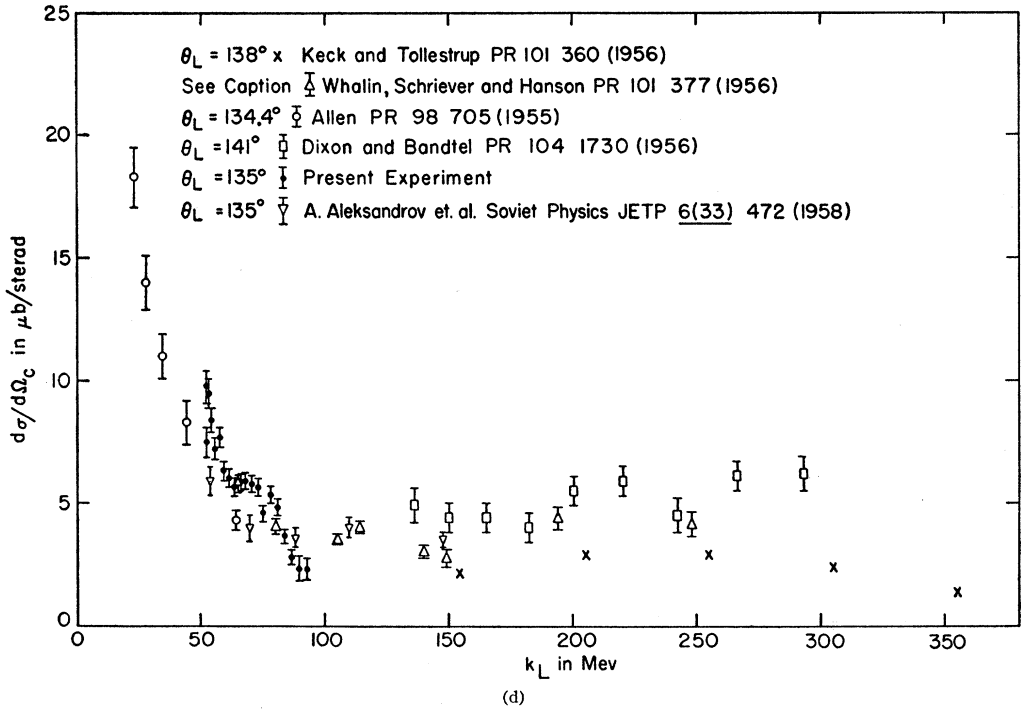

(d)

FIG. 4.—*Continued.*

particle-selector system. There is a natural separation into two types of the uncertainties affecting this experiment: (1) uncertainties which affect the shape of the angular distribution and (2) uncertainties which do not affect the angular distribution but only the total cross section. The major uncertainty of the first kind is the statistical uncertainty in the number of counts per channel, and the major uncertainty of the

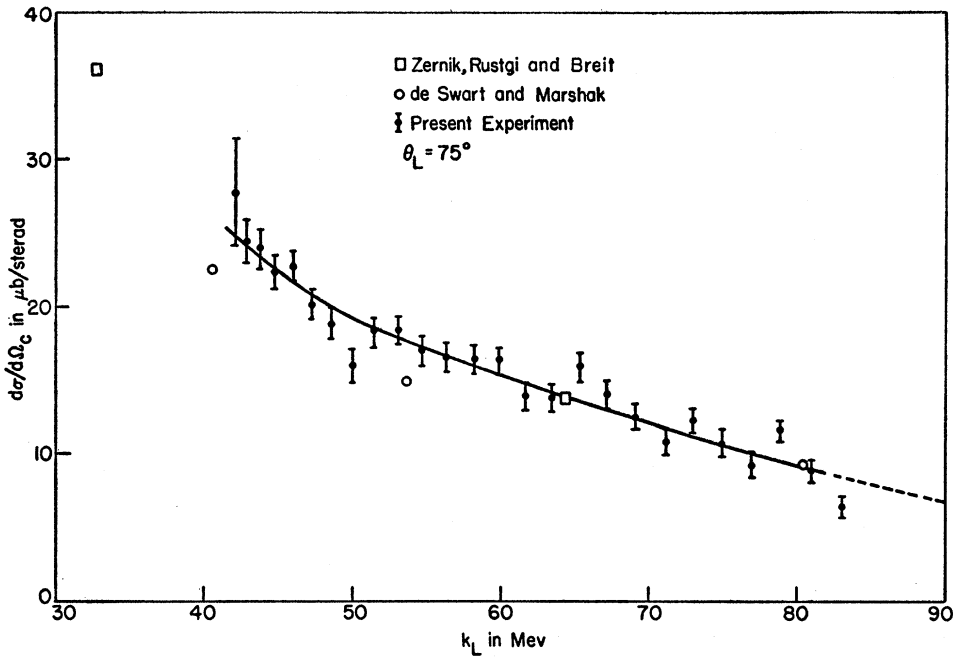

FIG. 5. A smoothed curve through the experimental points at 75°, along with the theoretical values of de Swart and Marshak and Zernik, Rustgi, and Breit.

second type is in the calibration of the Kerst-Edwards chamber.

IV. RESULTS AND CONCLUSIONS

A survey of experimental determinations of differential cross sections is given in Fig. 4. A striking feature of the status of experimental determinations of the differential cross section is the relatively small scatter in the determinations at the laboratory angle 90° compared to the scatter present in the experimental data for angles fore and aft of 90°. The agreement at 90° suggests that uncertainty in the determination of integrated photon fluxes is possibly not as serious as has been suspected. This, unfortunately, leaves one without a ready explanation of the discrepancies especially notable in the 45° and 135° results.

Angular Distributions

The dominant features of the angular distribution of photoprotons from deuterium in the medium and high-energy range are (1) the presence of a sizeable isotropic component in addition to a portion which as $\sin^2\theta_c$, which latter component is all that is predicted by calculations which assume that only central forces are operative in the n-p system,[16] and (2) an appreciable fore-aft asymmetry due to interference between the dominant electric dipole transitions and the electric quadrupole transitions. Initial attempts to account for the isotropic component in the angular distribution by taking into account the existence of noncentral forces in the n-p interaction were not too successful and led to investigations of the effect of virtual pion transitions.[17,18] More recently, however, work by Signell and Marshak,[19] Gammel and Thaler,[20] and Fischer, Pyatt, Hull, and Breit[21] has determined nucleon-nucleon potentials consistent with present experimental scattering data. Using potentials of this type calculations of the cross section for the deuteron photoeffect have been made by de Swart and Marshak,[11] Zernik, Rustgi, and Breit[12] and Nicholson and Brown.[22] The success of this work in predicting the amount of isotropic component experimentally observed seems to indicate that, at least in the intermediate energy range, virtual pion effects need not be introduced but that care must be

TABLE I. Values of the parameters a_0, a_1, a_2, and a_3 for the 135-Mev data of reference 5 and the 65- and 80-Mev data of reference 6,[a] in μb/sterad. k_l is in Mev.

Energy k_l	a_0	a_1	a_2	a_3	a^b	b^b	$\beta_1{}^b$	$\beta_2{}^b$
65	11.44	5.81	−6.54	−3.25	4.91	6.94	0.52	0.50
	0.56	1.2	0.99	1.8				
80	6.81	6.59	−1.18	−4.37	4.77	1.18	0.39	3.7
	0.42	0.93	0.81	1.4				
155	3.27	2.03	−1.38	−0.20	3.27	1.38	0.56	0.15
	0.15	0.46	0.51	0.94				

[a] The second entry in the second through fifth columns is the uncertainty estimate which is generated in the least-squares procedure.
[b] The values of a, b, β_1, and β_2 given here are obtained from a_0, a_1, a_2, and a_3 by the relations $a=a_0+a_2$, $b=-a_2$, $\beta_1=(a_1+a_3)/(a_0+a_2)$, and $\beta_2=a_3/a_2$.

[16] L. I. Schiff, Phys. Rev. **78**, 733 (1950); and J. F. Marshall and E. Guth, Phys. Rev. **78**, 738 (1950).
[17] N. Austern, Phys. Rev. **108**, 973 (1957).
[18] R. R. Wilson, Phys. Rev. **104**, 218 (1956); and F. Zachariasen, Phys. Rev. **101**, 371 (1956).
[19] P. S. Signell and R. E. Marshak, Phys. Rev. **106**, 832 (1957); and Phys. Rev. **109**, 1229 (1958).
[20] J. Gammel and R. Thaler, Phys. Rev. **107**, 291 (1957).
[21] Fischer, Pyatt, Hull, and Breit, Bull. Am. Phys. Soc. **3**, 183 (1958).
[22] A. F. Nicholson and G. E. Brown, Proc. Phys. Soc. (London) **73**, 221 (1959). This calculation is for $k_l=130$ Mev yielding $a=2.91$ microbarns per steradian, $b=0.69$ microbarn per steradian, and a total cross section of 42 microbarns.

taken because the results are sensitive to the D state probability in the initial state, the tensor force in the odd triplet state, and the hard core of the even singlet state.[23]

Analytic Forms for the Angular Distribution

The analytic form of the angular distribution suggested by de Swart and Marshak is

$$a(1+\beta_1\cos\theta_c)+b\sin^2\theta_c(1+\beta_2\cos\theta_c). \quad (1)$$

This is equivalent to the form suggested by Zernik, Rustgi, and Breit in their approximation E:

$$a+b\sin^2\theta+c\cos\theta_c+d\sin^2\theta_c\cos\theta_c+e\sin^2\theta_c\cos^2\theta_c, \quad (2)$$

except for the term in $\sin^2\theta_c\cos^2\theta_c$ in expression (2) which contributes of the order of one percent to the total cross section. A form which easily lends itself to a least squares fit to experimental data and which is equivalent to expression (1) is:

$$a_0+a_1\cos\theta_c+a_2\cos^2\theta_c+a_3\cos^3\theta_c, \quad (3)$$

a cubic in $\cos\theta_c$, where $a_0=a+b$, $a_1=a\beta_1+b\beta_2$, $a_2=-b$, and $a_3=-b\beta_2$. Under special conditions expressions (1) and (3) reduce to the forms which have previously been used for the synthesis of measured differential cross sections by experiments. It becomes the form used by references 1, 2, 3 and 6 when $\beta_1=\beta_2$. When $a_3=b\beta_2=0$, it becomes the form employed by references 5 and 7. These assumptions, however, are not consistent with the predictions of references 11 and 12 in the energy range in which their calculations were done. As a check on this point the values of the differential cross section for 155 Mev reported by reference 5 and those for 65 and 80 Mev reported by reference 6 were fitted

TABLE II. Values of the center-of-mass differential cross section.[a]

k_l	θ_c degrees	$d\sigma/d\Omega_c$	θ_c degrees	$d\sigma/d\Omega_c$	θ_c degrees	$d\sigma/d\Omega_c$	θ_c degrees	$d\sigma/d\Omega_c$
50	49.81	17.0	81.48	19.5	96.76	16.9	139.78	8.3
		0.6		0.6		0.25		0.5
55	50.03	15.8	81.81	17.2	97.08	14.6	140.00	7.5
		0.6		0.5		0.3		0.3
60	50.25	14.4	82.14	15.6	97.36	12.35	140.22	6.5
		0.6		0.6		0.3		0.2
65	50.46	13.2	82.43	13.6	97.67	11.0	140.43	5.9
		0.6		0.6		0.3		0.2
70	50.65	11.9	82.71	12.4	97.96	9.8	140.61	5.6
		0.6		0.5		0.3		0.2
75	50.84	10.45	82.97	10.7	98.24	8.9	140.81	5.15
		0.5		0.5		0.3		0.2
80	51.01	9.2	82.23	9.25	98.49	7.9	141.00	4.6
		0.5		0.5		0.2		0.2
85	51.18	8.1	83.48	8.0	98.74	6.5	141.17	3.8
		0.5		0.4		0.4		0.3
90	51.34	7.1	83.73	6.8	98.98	5.7	141.35	3.2
		0.5		0.6		0.6		0.3

[a] The second entry in alternate columns is the uncertainty associated with the quantity directly above it. These uncertainties do not include the effect of the uncertainty in the calibration of the Kerst-Edwards chamber. k_l is the laboratory photon energy in Mev. $d\sigma/d\Omega_c$ is given in units of μb/sterad.

[23] S. Hsieh, Progr. Theoret. Phys. (Kyoto) **21**, 585 (1959).

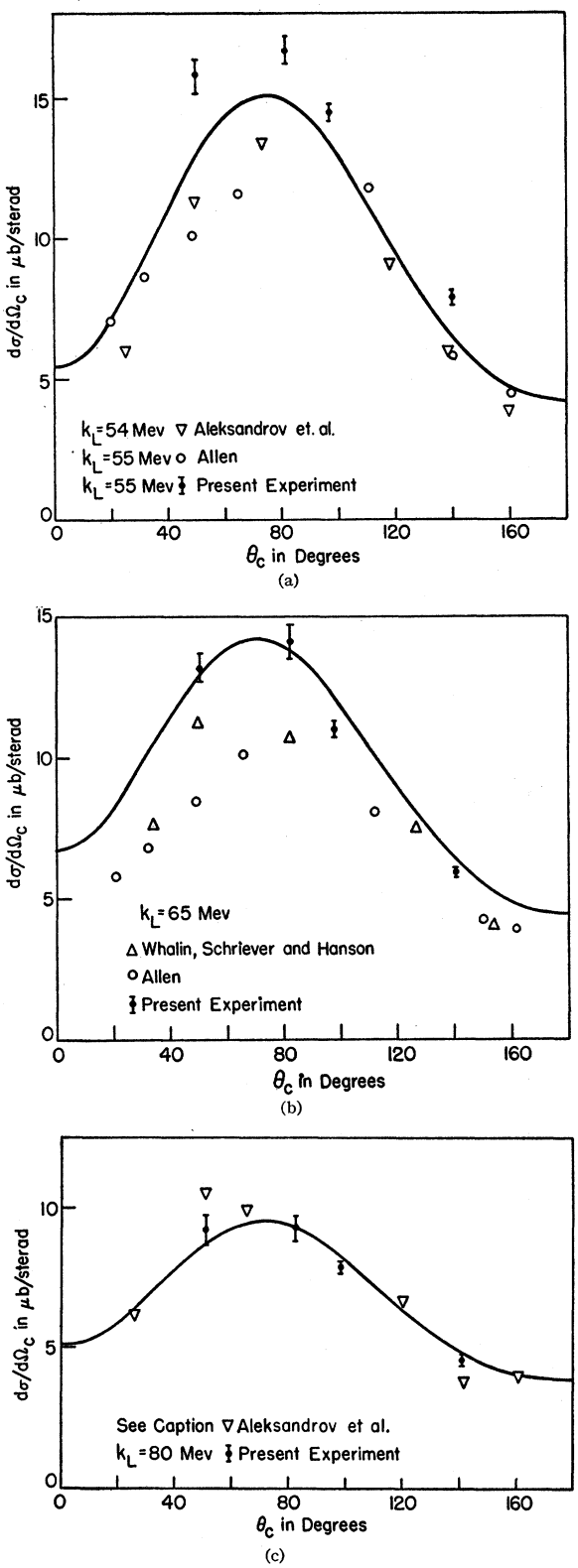

FIG. 6. Angular distribution plots: (a) the 53.7-Mev calculation of de Swart and Marshak; (b) the 64.4-Mev calculation of Zernik, Rustgi, and Breit in their approximation E; (c) the 80.4-Mev calculation of de Swart and Marshak. The values of Aleksandrov *et al.* are the averages of their 70- and 80-Mev values.

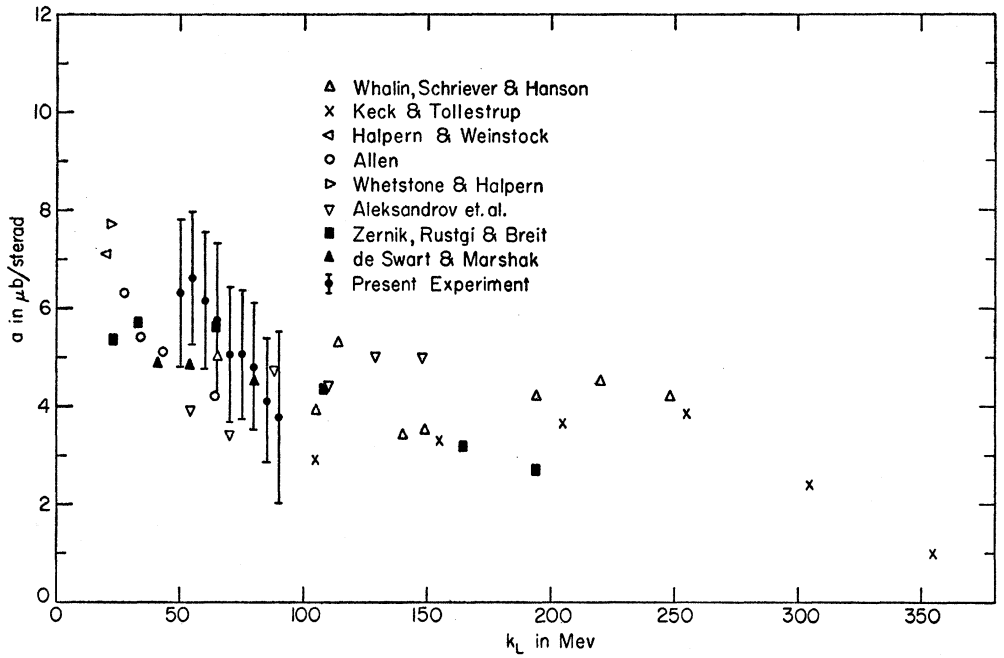

FIG. 7. The parameter *a versus* k_l: uncertainty estimates have been omitted for all points except those obtained in the present experiment to avoid the confusion introduced by their presence.

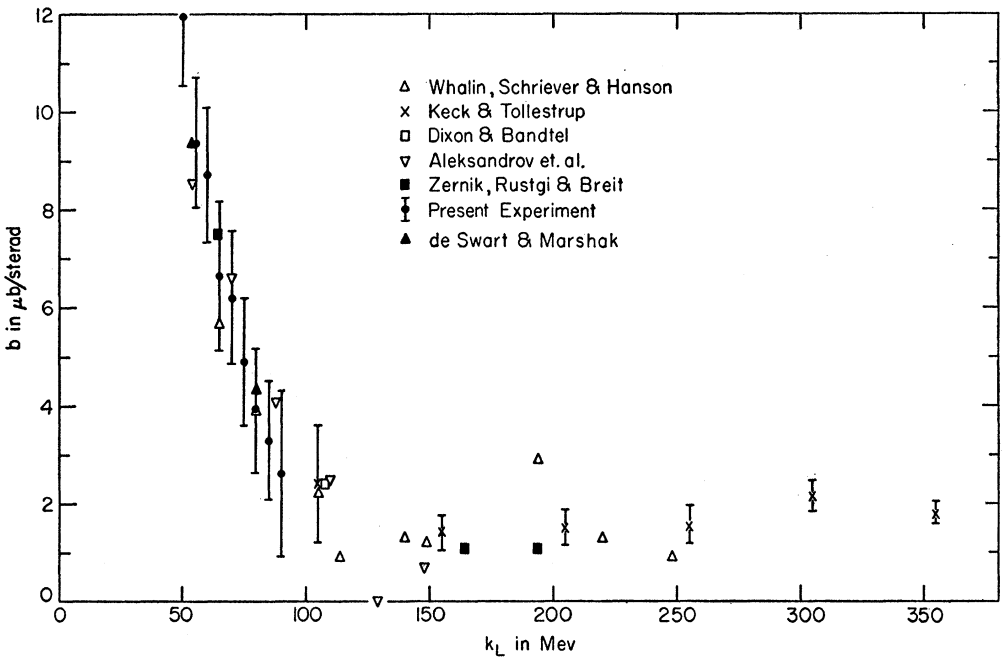

FIG. 8. The parameter *b versus* k_l.

by a least-squares procedure[24] with expression (3), yielding the results given in Table I.

Angular Distribution Parameters

In order to obtain estimates of the parameters entering into the analytic description of the angular distribution, values of the differential cross section for nine laboratory photon energies from 50 to 90 Mev in 5 Mev steps were taken from smooth curves drawn through the plots of the differential cross section *versus* k_1 for a fixed laboratory angle. It should be clearly understood that any presumption of monotonic variation of the differential cross section with energy has been disregarded in drawing these curves. However, even in the most extreme cases a strictly monotonic decrease with increasing energy could follow if the curve is relocated by amounts of at worst two times the estimated statistical uncertainty of the plotted

[24] F. T. Solmitz, internal report, University of Chicago (unpublished).

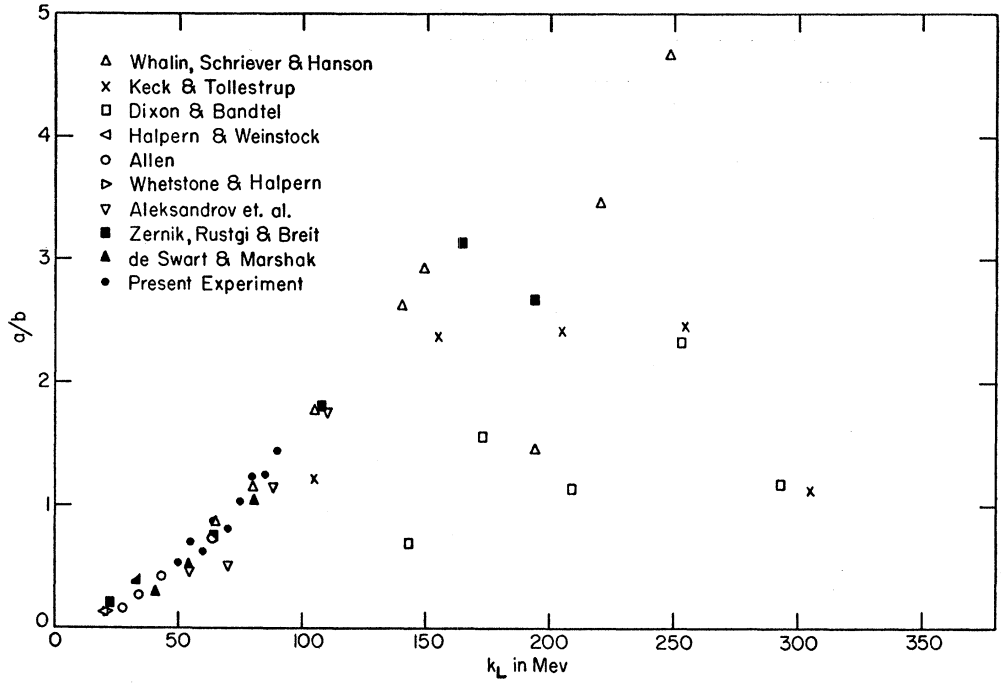

FIG. 9. a/b *versus* k_L.

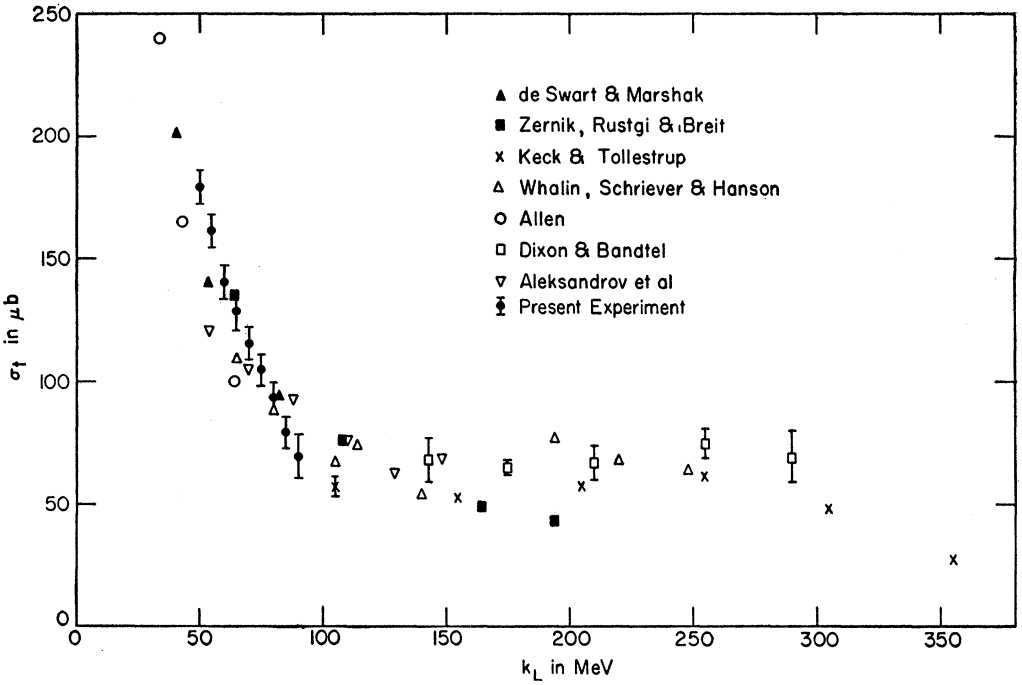

FIG. 10. The total cross section *versus* k_L.

points. A typical curve is shown in Fig. 5 along with the predictions of references 11 and 12. The values taken from these curves are given in Table II. The uncertainties indicated in Table II and subsequently used to determine the uncertainties in the parameters a_0, a_1, a_2, and a_3 were taken somewhat arbitrarily to be one-half those assigned to nearby values of the differential cross section calculated for each pulse-height analyzer channel.

Figure 6 presents the angular distributions predicted for 53.7 and 80.4 Mev by reference 11 and that predicted for 64.4 Mev by reference 12 in their approximation E along with various experimental results. In all three cases there is reasonable agreement as to the shape of

TABLE III. Values of the parameters a_0, a_1, a_2, a_3, and σ_t.[a]

E_l	a_0	a_1	$-a_2$	$-a_3$	σ_t
50	18.3	10.3	12.0	11.0	179
	0.3	2.4	1.4	5.1	7
55	16.0	10.2	9.4	10.7	162
	0.3	2.3	1.3	4.9	7
60	14.1	12.6	8.7	16.0	140
	0.3	2.2	1.4	4.7	7
65	12.4	10.0	6.6	11.2	128
	0.35	2.6	1.5	5.5	8
70	11.3	9.9	6.2	12.4	116
	0.3	2.0	1.4	4.3	7
75	9.95	6.8	4.9	7.3	104.5
	0.3	2.0	1.3	4.3	6.5
80	8.72	5.0	3.9	4.6	93
	0.25	1.7	1.3	3.8	6
85	7.4	5.6	3.3	5.9	79
	0.3	2.2	1.2	4.6	6
90	6.39	4.1	2.6	3.4	69
	0.4	1.0	1.7	6.8	9

[a] The second entry in every section of the table is the uncertainty associated with the first entry. a_0, a_1, a_2, and a_3 are in microbarns per steradian. σ_t is in microbarns. None of the uncertainties quoted here include the effect of the uncertainty in the calibration of the Kerst-Edwards chamber.

the angular distribution; however, particularly at 55 Mev there is considerable disagreement in the total cross section.

The results of fitting expression (3) to the differential cross sections given in Table II are given in Table III. Using the relationships $a=a_0+a_2$, $b=-a_2$, and $\sigma_t=(a_0+\frac{1}{3}a_2)$, Figs. 7, 8, 9, and 10 were obtained. The most striking features here is the agreement in both experimental and theoretical values of a/b up to approximately 100 Mev.

Although the large uncertainties in a_1 and a_3, as indicated in Table III, do not permit good estimates of the parameters, β_1 and β_2, occuring in expression (1), it is clear that $-a_3=b\beta_2$ is certainly larger than $a_1+a_2=a\beta_1$, and therefore that the fore-aft asymmetry indicated by the factor $(1+\beta_2\cos\theta_c)$ is appreciably larger than that indicated by the factor $(1+\beta_1\cos\theta_c)$, a conclusion which is in agreement with the predictions of references 11 and 12. It is, however, in disagreement with the results obtained in references 3 and 6 which were interpreted as being consistent with $\beta_1=\beta_2$ in the energy range from 20 to 65 Mev in reference 3 and from 60 to 250 Mev in reference 6. It is also reasonably certain that a_3 is a nonvanishing quantity in the energy range covered by this experiment. This latter conclusion is born out by the 65- and 80-Mev measurements of reference 6 as indicated in Table I.

It is also apparent from Figs. 7 through 10 that the study of the deuteron photoeffect is by no means in a final state. As was commented earlier, it is not obvious that the blame for existing experimental discrepancies can be ascribed to difficulties in the determination of photon flux. Ideally, one would hope that direct information on the nature of nucleon-nucleon forces could be obtained from experimental observation of the deuteron photoeffect. This does not seem, at least at present, to be possible in an unambiguous way.

ACKNOWLEDGMENTS

The author wishes to acknowledge the assistance and encouragement of Professor C. L. Oxley who suggested the problem, and the encouragement and advice of Professor S. K. Allison and Dr. A. S. Penfold. Thanks are also due for the advice given by Professor V. L. Telegdi and Dr. G. C. Morrison. Particular thanks are due to Mr. R. Gabriel for his assistance with the electronics employed in this experiment and for the efficient operation of the betatron. The aid of Mr. C. Bordeaux during the use of the cyclotron facility is very much appreciated. The services of the computer "George" at the Argonne National Laboratory through the kindness of Dr. W. Miller and Mr. S. Zawadski were an invaluable aid.